Distribution of charge cumulants of a chaotic quantum dot with nonideal contacts

F. A. G. Almeida, S. Rodríguez-Pérez, and A. M. S. Macêdo
Departamento de Física, Universidade Federal de Pernambuco, 50670-901 Recife, PE, Brazil
(Received 26 May 2009; revised manuscript received 18 August 2009; published 18 September 2009)

We performed numerical simulations of a quantum dot with nonideal contacts to obtain the probability distributions of transport observables associated with the first four charge-transfer cumulants (CTCs). For particular cases, several known results of the recent literature were recovered from our simulations, such as CTC distributions for systems with ideal contacts and CTC distributions for single-channel systems with contacts of arbitrary transparency. We analyze how CTC distributions are affected by a change in the number of open scattering channels in the leads and in the transparencies of the contacts. We found two remarkable features in the CTC distributions in the extreme quantum limit of a small number of open channels: an approximate similarity law for conductance distributions and the appearance of nonanalyticities in some CTC distributions. We interpret the appearance of these singularities by means of a geometrical argument and derive the exact values of the CTC at which the nonanalyticities in the corresponding distribution appear. Our simulations were performed via three different and independent algorithms, whose relative efficiencies are duly compared.

DOI: 10.1103/PhysRevB.80.125320 PACS number(s): 73.23.−b, 73.21.La, 05.45.Mt, 05.60.Gg

I. INTRODUCTION

In mesoscopic physics it is now well established that the quantum fluctuations of a transport observable, measured by the cumulants of its distribution, are just as informative as its average. This is particularly striking in charge-transfer phenomena, where temporal quantum fluctuations of the current have had many applications, such as measuring the charge of the carriers,[1,2] counting open transmission channels,[3] detecting entanglement[4] and many others. These temporal fluctuations are ultimately a direct consequence of the granularity of the transmitted charge, which may differ from the electronic unit of charge, e, in strongly correlated systems. The stochastic process characterizing this transmission deviates from the classical Poisson process because of the underlying quantum temporal correlations. An efficient way to characterize the stochastic quantum process of charge transfer is via the theory of full counting statistics,[5] which provides a generating function from which expressions for charge-transfer cumulants (CTCs) can be obtained. Using the Levitov-Lesovik formula,[5] the mth CTC can be written as

$$q_m = \sum_{i=1}^{N} f_m(\tau_i), \tag{1}$$

where f_m is a degree m polynomial given by

$$f_m(\tau) = \left. \frac{d^m}{dx^m} \ln[1 + \tau(e^x - 1)] \right|_{x=0}. \tag{2}$$

The set $\{\tau_i\}$ contains the nonzero eigenvalues of $\boldsymbol{tt}^\dagger$, $\boldsymbol{t}$ is the $N_1 \times N_2$ transmission matrix of the conductor, N_μ is the number of open channels in lead μ and $N \equiv \min(N_1, N_2)$.

The quantum interference phenomenon caused by the spatial coherence of the charge carriers induces mesoscopic sample to sample fluctuations of the measured current. This implies that each CTC, q_m, is an observable characterized by its own distribution. We have thus a very nontrivial statistical problem in which there are two sources of fluctuations with quite different natures: (i) the charge counting statistics, whose cumulants are characterized by the Levitov-Lesovic formula and (ii) the fluctuation of each CTC due to chaotic scattering inside the cavity. When the number of open channels is large, which corresponds to the semiclassical regime, i.e., $N \gg 1$, the distribution of any CTC tends to be approximately Gaussian[6,7] and consequently the average and the variance of the CTC give us most of the relevant information. However, in the extreme quantum limit (EQL), where $N \sim 1$, the system is nearly closed and the effect of quantum interference is substantially enhanced, thus making EQL an useful regime in which to understand nonperturbative quantum effects in mesoscopic transport. Furthermore, since there are strong CTC fluctuations in EQL, the average and the variance of the CTC are insufficient to describe the system. Consequently, we need to know the full CTC distributions which may be quite broad and contain irregularities such as nonanalyticities. For ideal contacts, these irregular distributions have been predicted theoretically[8,9] and observed experimentally[10] in quantum dots. In addition, the nonanalyticities of the CTC distributions are important to understand the metal-insulator crossover in quasi-one-dimensional disordered wires.[11–14]

A setup for studying electronic quantum transport through a nanostructure can be modeled as a type of electrical circuit by dividing it in connectors, nodes and reservoirs.[15] Reservoirs are described by equilibrium distribution functions and serve as source and drain to the physical current. The connectors are characterized by a set $\{\tau_i\}$ of transmission coefficients for each active scattering channel and may represent barriers or quantum point contacts. These two elements model the parts of the circuit that can be controlled by the experimentalist. Nodes, on the other hand, are characterized by uncontrollable phase shifts due to disorder (or chaos in ballistic quantum dots). So, the hardest technical step in calculating any transport quantity is to eliminate the irrelevant small scale degrees of freedom affected by the disorder and keep only the relevant large scale modes. There are many techniques that can handle such a difficulty, viz., the Keldysh

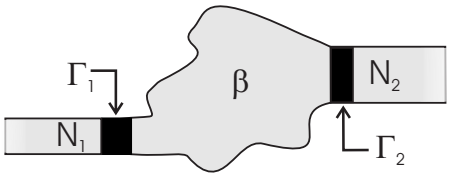

FIG. 1. Schematic view of a chaotic quantum dot with two leads. Each lead is characterized by the number of open channels N_1 and N_2. Γ_1 and Γ_2 are the barriers' transparency. The physical symmetries of the electron dynamics inside the chaotic cavity is indexed by β.

quasiclassical Green's function approach,[15] the diagrammatic perturbative expansion of the unitary group[16,17] and the supersymmetric nonlinear sigma model.[18,19] However, only few of them can access the nonperturbative regime characterized by the EQL. In this regime, statistical properties of charge-transfer cumulants have been obtained for quantum dots coupled ideally to electron reservoirs using both random-matrix theory (RMT) (Refs. 8 and 16) and Selberg's integral.[9,20,21] Inspired by recent work on the weak-localization correction of the shot-noise power,[22] we expect that the introduction of barriers of arbitrary transparency should affect qualitatively the interplay between the spatial and the temporal coherences in the dot and therefore the systems' CTC statistics. This is the main conceptual motivation for our numerical simulations.

In this work we consider a quantum dot coupled to two electron reservoirs through nonideal contacts of arbitrary transparencies and with only a few open scattering channels, see Fig. 1. The dwell time of the electrons in the dot is assumed to be much bigger than both the Ehrenfest time and the ergodic time, so that the cavity can be considered to be in a universal chaotic regime and the use of random-matrix theory can be justified. We employ three different numerical techniques to generate the CTC statistics and their relative efficiencies are carefully compared. We study the effects of varying the transparency of the barriers in the CTC distributions for the three standard Wigner-Dyson (WD) ensembles.[23,24] We observe several nonanalyticies in the CTC distributions, which we explain, following Ref. 9, with a simple geometrical argument. We also determine the special values of the CTC at which these singularities appear. We believe that the occurrence of these special features in the CTC distributions in the EQL is an important universal feature of mesoscopic quantum transport.

This paper is organized as follows. In Sec. II we present a brief description of two equivalent RMT techniques:[25–28] the Hamiltonian approach and the scattering matrix formalism. In Sec. III we explain how to implement three different numerical algorithms based on these two approaches. We also present results for the distributions of the first four CTC. In order to explain the nonanalyticity in the CTC distributions, we generalize the geometrical argument of Ref. 9 in Sec. V. A summary and conclusions are presented in Sec. VI.

II. RANDOM-MATRIX TECHNIQUES

For the calculations of the CTC distributions, we need to generate numerically with great efficiency the scattering matrix $\boldsymbol{S}$ of an open chaotic quantum dot connected to two ideal leads by nonideal contacts. As we show below, this can be done basically through two different approaches.

A. Hamiltonian approach

The Hamiltonian matrix $\boldsymbol{H}$ used to model the dynamics of noninteracting particles in the ballistic chaotic cavity[26] is usually taken to be a member from the Gaussian random matrix ensemble with probability distribution given by

$$P(\boldsymbol{H}) = \mathcal{N} \exp\left[-\frac{\beta}{4C} \mathrm{tr}(\boldsymbol{H}^2) \right], \tag{3}$$

where $\mathcal{N}$ is a normalization factor, $C=\lambda^2/M$, M is the number of resonances inside the cavity, λ is a variance related parameter and $\beta=1$ (GOE), 2 (GUE), or 4 (GSE) is a universality index accounting for the presence or the absence of fundamental physical symmetries in the electron dynamics inside the cavity, such as time-reversal and spin-rotation invariances.[23] A crucial feature of this approach is that the limit $M \to \infty$ must to be taken in the end of the calculation to assure the universality of the observables, such as the CTC distributions. The scattering matrix is constructed using the formula

$$\boldsymbol{S}(E) = \boldsymbol{I}_{N_T} - 2\pi i \boldsymbol{W}^\dagger \frac{1}{E\boldsymbol{I}_M - \boldsymbol{H} + i\pi \boldsymbol{W}\boldsymbol{W}^\dagger} \boldsymbol{W}. \tag{4}$$

Here $\boldsymbol{W}$ is an $M \times N_T$ coupling matrix that contains information about the total number of open channels $N_T=N_1+N_2$ in the two leads, the mean level spacing in the cavity and the transparencies of the barriers. It can be separated into two parts: an $M \times N_1$ matrix $\boldsymbol{W}_1$ and an $M \times N_2$ matrix $\boldsymbol{W}_2$ as follows:

$$\boldsymbol{W} = (\boldsymbol{W}_1 \ \ \boldsymbol{W}_2) \tag{5}$$

In order to neglect direct processes such as a prompt transmission from one lead to the other without forming an intermediate resonant state, we impose the following orthogonality condition:[26,27]

$$\boldsymbol{W}_\mu^\dagger \boldsymbol{W}_\nu = \boldsymbol{\omega}_\mu \frac{M\Delta}{\pi^2} \delta_{\mu,\nu}, \tag{6}$$

where Δ is the mean level spacing in the dot and $\boldsymbol{\omega}_\mu$ is a diagonal matrix given by

$$\boldsymbol{\omega}_\mu = \mathrm{diag}(\omega_{\mu,1}, \omega_{\mu,2}, \ldots, \omega_{\mu,N}), \tag{7}$$

which is related to the transmission probability $\Gamma_{\mu,j}$ of the channel j in the lead μ by the relations

$$\alpha_{\mu,j} \equiv -\ln(\omega_{\mu,j}),$$

$$\Gamma_{\mu,j} = \mathrm{sech}^2(\alpha_{\mu,j}/2). \tag{8}$$

This model provides a stochastic description of electron transfer through a chaotic ballistic cavity coupled to two reservoirs via imperfect contacts, i.e., barriers of arbitrary transparencies. In the next section, we present an alternative but equivalent approach that has some advantages from a numerical efficiency point of view.

B. Scattering matrix formalism

It is also possible to construct the scattering matrix of the double barrier quantum dot by a composition of the scattering matrices of the barriers and the scattering matrix of the cavity. Following Ref. 28, we employ the stub parametrization

$$\boldsymbol{S} = \bar{\boldsymbol{S}} + \boldsymbol{T}'(\boldsymbol{I}_{N_T} - \boldsymbol{S}_0\boldsymbol{R}')^{-1}\boldsymbol{S}_0\boldsymbol{T}. \tag{9}$$

Here

$$\bar{\boldsymbol{S}} = \begin{pmatrix} \boldsymbol{r}_1 & 0 \\ 0 & \boldsymbol{r}_2 \end{pmatrix}, \tag{10}$$

where $\boldsymbol{r}_\mu$ is the $N_\mu \times N_\mu$ reflection matrix of the contact μ, $\boldsymbol{S}_0$ is an $N_T \times N_T$ random matrix belonging to a circular ensemble [circular orthogonal ensemble (COE), circular unitary ensemble (CUE), or circular symplectic ensemble (CSE)][23] which represents the scattering matrix of the cavity connected to the leads via ideal contacts.[25] $\boldsymbol{R}'$, $\boldsymbol{T}'$, and $\boldsymbol{T}$ are $N_T \times N_T$ matrices chosen in such a way that the matrix

$$\boldsymbol{\Sigma} = \begin{pmatrix} \bar{\boldsymbol{S}} & \boldsymbol{T}' \\ \boldsymbol{T} & \boldsymbol{R}' \end{pmatrix} \tag{11}$$

is unitary, symmetric or unitary self-dual, depending on the symmetry of the ensemble. This parametrization redundancy is due to the fact that $\boldsymbol{S}$ is distributed according to the Poisson kernel[29]

$$P(\boldsymbol{S}) \propto |\det(\boldsymbol{I}_{N_T} - \bar{\boldsymbol{S}}^\dagger \boldsymbol{S})|^{-(\beta N_T + 2 - \beta)} \tag{12}$$

and thus, by specifying $\bar{\boldsymbol{S}}$ and β we have sufficient information to determine the statistical properties of any transport observable of the system.

Alternatively, the transfer matrix $\boldsymbol{M}$ of the composite dot-barriers system[29] can be obtained from a simple multiplicative rule, i.e., the product of the transfer matrices of each object separately, viz., the first barrier, the quantum dot and the second barrier, as follows:

$$\boldsymbol{M} = \boldsymbol{M}_1 \boldsymbol{M}_{\mathrm{dot}} \boldsymbol{M}_2. \tag{13}$$

Since the scattering matrix of any object can always be written in block form as

$$\boldsymbol{S} = \begin{pmatrix} \boldsymbol{r} & \boldsymbol{t}' \\ \boldsymbol{t} & \boldsymbol{r}' \end{pmatrix} \tag{14}$$

the corresponding transfer matrix can be obtained using the following transformation rule:

$$\boldsymbol{M} = \begin{pmatrix} (\boldsymbol{t}^\dagger)^{-1} & \boldsymbol{r}'(\boldsymbol{t}')^{-1} \\ -(\boldsymbol{t}')^{-1}\boldsymbol{r} & (\boldsymbol{t}')^{-1} \end{pmatrix}. \tag{15}$$

In the next section we shall present three different numerical methods, based on the Hamiltonian and the scattering matrix approaches, to generate realizations of the charge-transfer cumulants.

III. NUMERICAL SIMULATIONS

Using three distinct algorithms, described below, based on the Hamiltonian and the scattering matrix formalisms discussed in the previews section, we show results from numerical simulations of a ballistic chaotic cavity coupled nonideally to electron reservoirs and belonging to each one of the WD ensembles. A comparison of the relative efficiency of these three algorithms is presented in Appendix A.

A. Scattering matrix ensembles

We shall now describe how we have constructed the realizations of the random scattering matrix ensembles which were used in our numerical simulations. We shall assume for simplicity that all scattering channels have the same transmission probability $\Gamma_{\mu,j} = \Gamma_\mu$. For the case of symmetric leads we use the notation $\Gamma \equiv \Gamma_1 = \Gamma_2$ and $N = N_1 = N_2$.

1. Hamiltonian formalism

Since we aim at predictions for realistic chaotic systems, only universal local in spectrum features will be considered.[19] Consequently, we neglect the energy dependence of the scattering matrix by setting $E=0$ and in addition we impose universality by implementing Dyson's scaling limit. The $\boldsymbol{H}$ elements can be real numbers (GOE), complex numbers (GUE), or real quaternions (GSE) and are determined by β real random Gaussian variables in each case $\{H_{i,j}^{(n)}\}_{n=0}^{\beta-1}$. In order to satisfy Eq. (3), we have demanded the following correlations:

$$\langle H_{i,j}^{(n)} \rangle = 0,$$

$$\langle H_{i,j}^{(n)} H_{k,l}^{(m)} \rangle = \delta_{n,m}\delta_{i,k}\delta_{j,l} \times C[\delta_{i,j}(2\delta_{n,0} - \beta^{-1}) + \beta^{-1}]. \tag{16}$$

The coupling matrices $\boldsymbol{W}_{\boldsymbol{\mu}}$ can be constructed by taking advantage of the orthogonality relations of the discrete Fourier basis. So, we have adopted the following parameterization:

$$(W_\mu)_{j,k} = e^{-\alpha_\mu/2} \sqrt{\frac{2\lambda}{\pi(M+1)}} \sin\left[\frac{j(N_1\delta_{\mu,2} + k)\pi}{M+1}\right], \tag{17}$$

which is in accordance with Eq. (6) due to the asymptotic relation $M\Delta = \pi\lambda$ for $M \gg 1$.

Therefore, with a numerical routine that samples Gaussian random numbers we can obtain realizations of the random scattering matrix of the system by means of the Mahaux-Weidenmüller (MW) formula (4). We may thus call this procedure the MW method.

2. Scattering formalism

In this approach we use the Hurwitz parameterization[30,31] to generate random unitary matrices $\boldsymbol{S}_0^u = \boldsymbol{U}$ belonging to the CUE. Random matrices from the COE can be parametrized in terms of CUE random matrices $\boldsymbol{U}$ as follows:

$$\boldsymbol{S}_0^o = \boldsymbol{U}^T\boldsymbol{U}, \tag{18}$$

where T stands for the transposition operation. For matrices from the CSE, we have

$$\boldsymbol{S}_0^s = \boldsymbol{U}^D\boldsymbol{U}, \tag{19}$$

where the superscript D indicates the quaternion duality operation.

The scattering matrices of the contacts can be written in block form as

$$\boldsymbol{S}_{\mu} = \begin{pmatrix} \boldsymbol{r}_{\mu} & \boldsymbol{t}'_{\mu} \\ \boldsymbol{t}_{\mu} & \boldsymbol{r}'_{\mu} \end{pmatrix} \tag{20}$$

where $\boldsymbol{r}_{\mu}$, $\boldsymbol{r}'_{\mu}$, $\boldsymbol{t}_{\mu}$, and $\boldsymbol{t}'_{\mu}$ are $N_{\mu}\times N_{\mu}$ matrices which we assume to be given by

$$\boldsymbol{r}_{\mu} = \boldsymbol{r}'_{\mu} = \sqrt{1-\Gamma_{\mu}}\boldsymbol{I}_{N_{\mu}},$$

$$\boldsymbol{t}_{\mu} = \boldsymbol{t}'_{\mu} = i\sqrt{\Gamma_{\mu}}\boldsymbol{I}_{N_{\mu}}, \tag{21}$$

where $\boldsymbol{I}_{N_{\mu}}$ is a unit matrix. We have implemented two procedures, based on the scattering formalism, to concatenate the cavity to the leads via nonideal contacts. The first one, denoted the stub (ST) method, is based on the parameterization Eq. (9). Accordingly, we have chosen $\boldsymbol{R}'=\bar{\boldsymbol{S}}$ and

$$\boldsymbol{T} = \boldsymbol{T}' = \begin{pmatrix} \boldsymbol{t}_1 & 0 \\ 0 & \boldsymbol{t}_2 \end{pmatrix}. \tag{22}$$

The other procedure is the transfer matrix (TM) method, in which the scattering matrices of the cavity and the barriers are converted into transfer matrices by the transformation, Eq. (15), and using the multiplication law, Eq. (13), the global $\boldsymbol{M}$ is calculated, yielding the global $\boldsymbol{S}$ by the inverse conversion.

B. Sampling

We have performed samplings of the first four CTC from the numerical realizations of the random scattering matrix. From these samplings we extracted the CTC distributions for arbitrary barrier transparencies, number of open scattering channels and WD classes. We remind the reader that the first CTC is the dimensionless conductance $g=q_1$, the second is the dimensionless shot-noise power $p=q_2$, the third and the fourth CTC are denoted q_3 and q_4, respectively. From Eq. (1) we have the explicit expressions

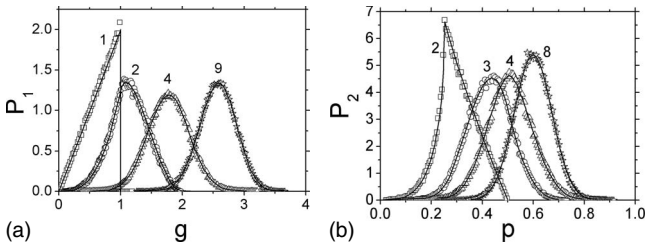

FIG. 2. Distributions of the conductance, g, and shot-noise power, p, of a quantum dot with ideal contacts. The numbers labeling the curves are values of N_2, while $N_1=4$ for both graphs. We used $\beta=1$ for P_1 and $\beta=2$ for P_2. The scatter is the simulation data and the solid lines are exact results (Ref. 9).

$$f_1(\tau) = \tau,$$

$$f_2(\tau) = \tau(1-\tau),$$

$$f_3(\tau) = \tau(1-\tau)(1-2\tau),$$

$$f_4(\tau) = \tau(1-\tau)(1-6\tau+6\tau^2). \tag{23}$$

Our main focus in this work is the extreme quantum regime (small number of scattering channels), where to the CTC distributions are broad and exhibit nonanalytical features, which are in sharp contrast with the Gaussian profiles found for a large number of open channels and with ideal contacts,[9] although nonanalytic points have been found in this regime as well.[6]

Before analyzing our results let us compare the simulations with known exact results from the literature. In Fig. 2 we compare our data with exact analytical results for the distributions of the conductance and the shot-noise power of a ballistic chaotic cavity with two ideal contacts.[9] Note the excellent agreement in all curves. For a chaotic quantum dot with a single nonideal contact, Ref. 32 gives an exact integral representation for the distribution of the transmission

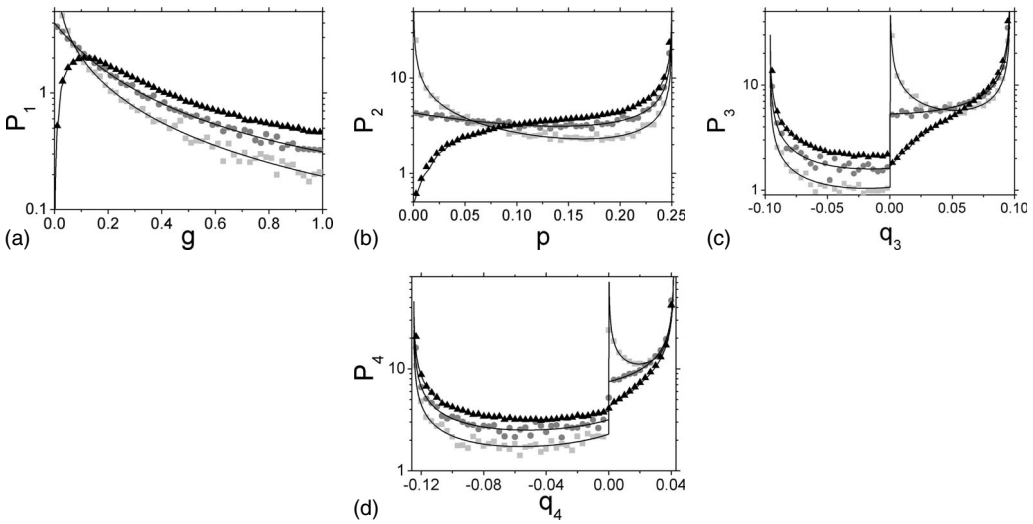

FIG. 3. Distributions of the first four CTC for a single-channel chaotic quantum dot with barriers' transparency $\Gamma=2/3$ and $\beta=1$, 2, and 4. The scatter is the simulation data and the solid lines are exact results (Ref. 32). All vertical axis are logarithmically scaled.

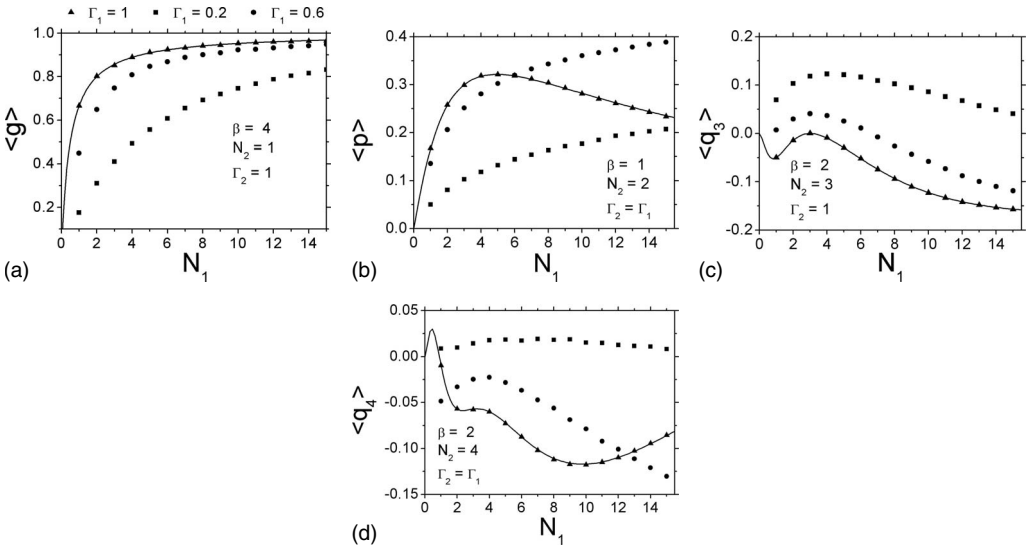

FIG. 4. Averages of the first four CTC versus N_1 for various values of N_2, Γ_1, Γ_2, and β. The scatter is the simulation data and the solid lines are guides to eyes of the exact results for ideal contacts (Refs. 8 and 19).

probability, $\rho(\tau)$, for all three WD ensembles. Using this result, the exact distributions of the CTC can be obtained [see Eq. (24) with $N=1$]. In Fig. 3 we compare these exact results with our simulations and an excellent agreement can again be observed. Furthermore, exact integral expressions for the statistical characteristics (average and variance) of the first two CTC for imperfect multichannel contacts have been recently obtained using the supersymmetry method for both the orthogonal and unitary ensemble,[33] which are also found to be in perfect agreement with our simulation.

Let us now consider some illustrative examples of the results. In Fig. 4 we show data from our simulations for the average CTC of a quantum dot with two nonideal contacts under various conditions. The analytical results for ideal contacts obtained in Refs. 8 and 19 are shown as solid lines in the panels. In Fig. 5, we illustrate the typical dependence of the average CTC on the barriers' transparencies, which are always continuous and smooth functions. The CTC distributions for nonideal contacts with number of channels dependence are showed in Fig. 6. We emphasize the tendency to Gaussian shape as the number of channels increases. This feature is also present in systems with ideal contacts as we can see in Fig. 2. Finally, in Fig. 7 we illustrate the behavior of the CTC distribution functions, more specifically the third and the fourth CTC, as a function of the barrier transparency. Note the disappearance of the Gaussian shape as the barrier transparency decreases. In Secs. IV and V we shall describe some striking features of the CTC distributions in the extreme quantum limit, namely, a similarity law for conduc-

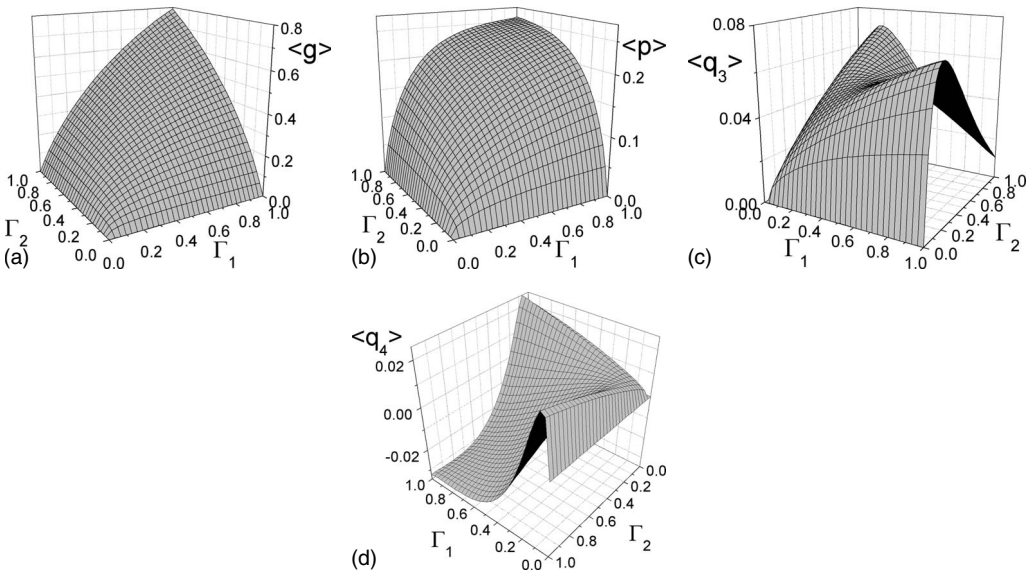

FIG. 5. Ensemble average of the first four charge-transfer cumulants versus Γ_1 and Γ_2 for a chaotic quantum dot with two scattering channels in each lead and $\beta=1$.

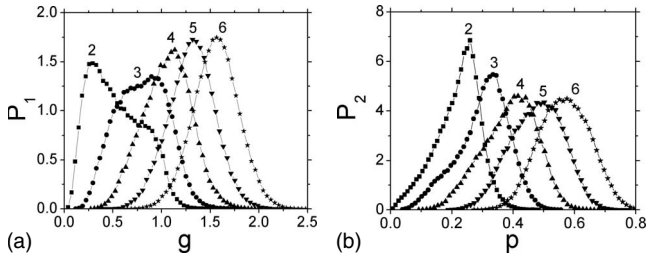

FIG. 6. Distributions of the conductance, g, and shot-noise power, p, of a quantum dot with symmetric leads, barriers' transparency $\Gamma=0.5$ and $\beta=4$. The numbers labeling the curves are values of the number of channels in each lead.

tance distributions and the appearance of nonanaliticities in some CTC distributions.

IV. SIMILARITIES BETWEEN CONDUCTANCE DISTRIBUTIONS

The decrease in the average conductance as the number of channels, N, or the barriers' transparency, Γ, reduces is physically quite intuitive, because increasing N or Γ enhances the transmission probability which in turn increases the average conductance. More specifically, let $\langle g\rangle_{N,\Gamma}$ denote the average conductance, then from the argument above if we fix N and Γ we can always find for each N' a physically meaningful value for Γ' such that $\langle g\rangle_{N,\Gamma}=\langle g\rangle_{N',\Gamma'}$. As a concrete example consider the semiclassical limit, where the average conductance is given by Ohm's composition law of two identical resistors in series, with resistance $R=1/(N\Gamma)$, therefore $\langle g\rangle=1/(2R)=N\Gamma/2$ and thus $\Gamma'=N\Gamma/N'$. Nevertheless, the average is just the first moment of a distribution and it would be interesting to investigate whether this rescaling extends to the full conductance distribution.

We proceed by fixing N and Γ, setting $N'>N$, and varying $\Gamma'<\Gamma$. We observed that provided N' is sufficiently close to N some remarkable similarities between the conductance distributions emerged. Using the notation (N,Γ), Fig. 8 shows strong similarities between the conductance distribution for the pairs $\{(3,0.63),(2,1)\}$, $\{(3,0.31),(1,1)\}$, and $\{(2,0.46),(1,1)\}$ which suggest an approximate scaling law for the conductance distribution

$$P_1(g;N,\Gamma) \simeq P_1(g;N',\Gamma'=N\Gamma/N')$$

with N' close to N. Note that the relation $\Gamma'=N\Gamma/N'$ is reminiscent of Ohm's law. We did not find similar approximate scaling laws for the other CTC distributions.

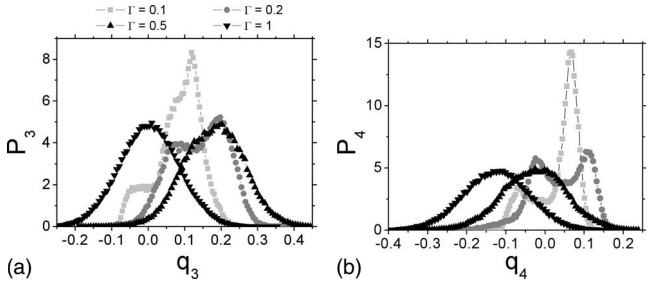

FIG. 7. Distributions of the third and fourth CTC of a chaotic quantum dot with $\beta=1$, eight scattering channels in each lead and barriers of transparency Γ.

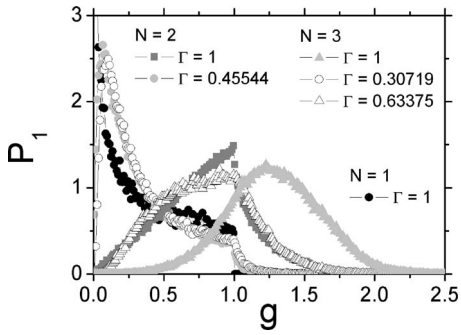

FIG. 8. Conductance distributions for symmetric chaotic quantum dots with $\beta=1$. Each distribution is characterized by the parameters (N,Γ). Note the similarities between distributions for certain systems with different (N,Γ). The values for the nonideal transparencies $(\Gamma\neq 1)$ were estimated by the minimization of the distance between the distributions, which was quantified by means of the relative entropy (Ref. 34).

V. NONANALYTICITIES IN THE CTC DISTRIBUTIONS

The presence of nonanalyticities in the CTC distribution for ideal contacts has been noticed before in the literature.[8,9,11–14] We show in Fig. 9 our results for the first four CTC distributions for a double channel chaotic cavity with symmetric barriers in the orthogonal ensemble and for several values of the barrier transparency. The presence of nonanalytic points is clearly visible. In Ref. 9 a geometrical interpretation was presented for the positions of the nonanalyticities in the distributions of the first two CTC. In this section, we generalize this idea for any CTC distribution and calculate the positions of all nonanalyticities.

Our starting point is the general formula for the distribution of the mth order CTC, q_m, which is given by

$$P_m(q_m) = \int_C d\vec{\tau}\rho(\vec{\tau})\delta\left(q_m - \sum_{i=1}^{N} f_m(\tau_i)\right) \tag{24}$$

where we abbreviated $\vec{\tau}\equiv\{\tau_i\}$, C denotes the N-dimensional hypercube of edge length 1 and $\rho(\vec{\tau})$ is the joint distribution of transmission eigenvalues. The two factors in the integrand of Eq. (24) carry very different types of physical information. The joint distribution of transmission eigenvalues contains all the statistically relevant physical information about the system including the transparencies of the barriers and all the effects of the underlying chaotic dynamics. The δ function, on the other hand, does not express any physical feature of the system except for the number of open channels N. Geometrically, Eq. (1) describes a hypersurface in $\mathbb{R}^{N+1}$ if we take q_m as an additional variable or a hypersurface in $\mathbb{R}^N$ if we fix the value of q_m. We will refer to these geometrical objects as $HS_{N+1}^{(m)}$ and $HS_N^{(m)}$ for the first and the last case, respectively. Differently from $HS_{N+1}^{(m)}$ which has just a single branch, $HS_N^{(m)}$ can have several branches which can be truncated by the N-dimensional hypercube $0\leq\tau_i\leq 1$. For the first two CTC, $HS_N^{(1)}$ and $HS_N^{(2)}$ are represented by families of hyperplanes and hyperspheres, respectively. However, for

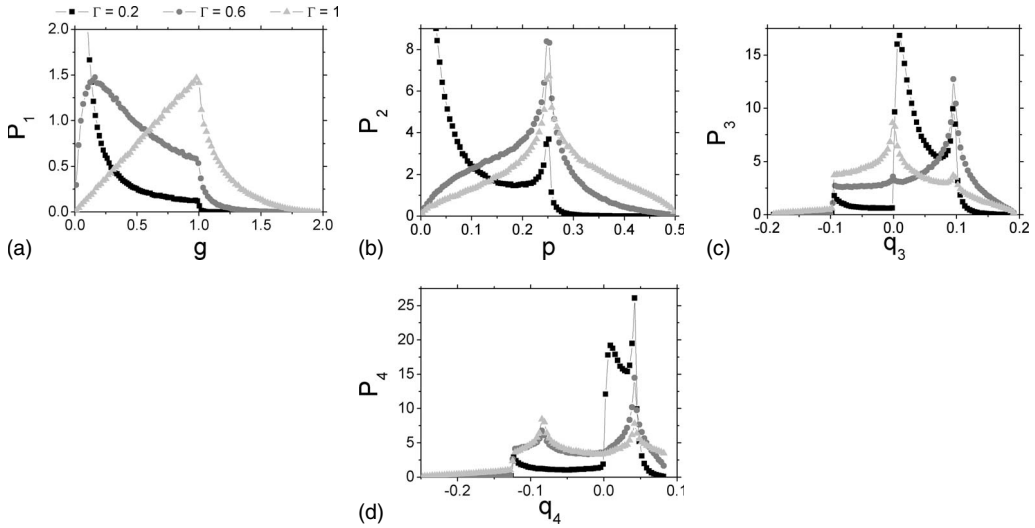

FIG. 9. Distributions of the first four CTC for a chaotic quantum dot in the orthogonal WD ensemble with two scattering channels in each lead and barriers' transparency $\Gamma=0.2$, 0.6, and 1.

$m>2$ there is an intricate variety of geometrical shapes as the value of q_m is varied. In Fig. 10 we show the curves $HS_2^{(3)}$ and $HS_2^{(4)}$ determined by some fixed values of q_3 and q_4, respectively. Note that in some regions the curves are truncated by the unit square represented by the area shown in the figures. In the case of q_3, $HS_2^{(3)}$ starts as a dot at the minimum of $HS_{2+1}^{(3)}$, located in the intersection of the loops in the right upper part of Fig. 10(a). Increasing q_3 it reaches a configuration with two saddle points of $HS_{2+1}^{(3)}$ and then it collapses to a dot at the maximum of $HS_{2+1}^{(3)}$, located in the left lower part of Fig. 10(a), through a series of shrinking loops. Similarly, for the fourth CTC, $HS_2^{(4)}$ starts as a dot at the minimum of $HS_{2+1}^{(4)}$ in the center of the square, reaches a configuration containing four saddle points of $HS_{2+1}^{(4)}$, and finally it evolves toward four dots at the maxima of $HS_{2+1}^{(4)}$, which are located near the corners of the square.

In order to distinguish between the possible causes of the nonanalitycities, we define the following "geometrical" distribution function:

$$P_m^G(q_m) \equiv \left|\frac{dV_G}{dq_m}\right| = \left|\frac{d}{dq_m}\int_C d\vec{\tau}\theta\left(q_m - \sum_{i=1}^{N} f_m(\tau_i)\right)\right|, \tag{25}$$

where V_G is the volume limited by the hypersurface $HS_N^{(m)}$.

Let us start our analysis with the first CTC, the conductance. When g increases the hyperplane $HS_N^{(1)}$ translates in $\mathbb{R}^{N+1}$. When it crosses a vertex of the hypercube $0\leq\tau_i\leq 1$, $V_G(g)$ changes its slope which in turn generates a discontinuity in $P_1^G(g)=|dV_G(g)/dg|$. Therefore, the conductance distribution, $P_1(g)$, exhibits (possibly weak) nonanalyticities at $g=\kappa$, with $0<\kappa\leq N$ in agreement with Ref. 9.

Consider now the CTC with $m>1$. The vertices of the hypercube can cause nonanalyticities only at $q_m=0$ because when $m>1$ we have the following property:

$$f_m(1) = f_m(0) = 0. \tag{26}$$

In addition to the vertices of the hypercube, we observed two kinds of singular situations in which the second derivative of V_G does not exist. The first one occurs when $HS_N^{(m)}$ passes through an extreme or a saddle point in $HS_{N+1}^{(m)}$. This kind of singularity is analogous to the *Van Hove singularities* in the density of electronic states of a crystalline solid.[35] The second one corresponds to the situations when $HS_N^{(m)}$ touches a boundary of the hypercube different from a vertex (see Fig. 10). In the first case, the nonanalytic points are found by demanding the gradient vector field of the hypersurface to vanish. In the second one, the gradient is perpendicular to the vectors that generate the boundaries of the hypercube (excluding vertices), i.e., edges, faces, cubes, tesseracts, etc. Note that as the dimension N of the hypercube increases by one, there is another element which could be touched. So, singularities of this kind are inherited as we move from N to $N+1$ open channels.

Let us now be more specific. We start with the simple case $N=1$, in which Eq. (1) defines a continuous set of points given by $q_m=f_m(\tau)$. Equation (26) can then be expressed as

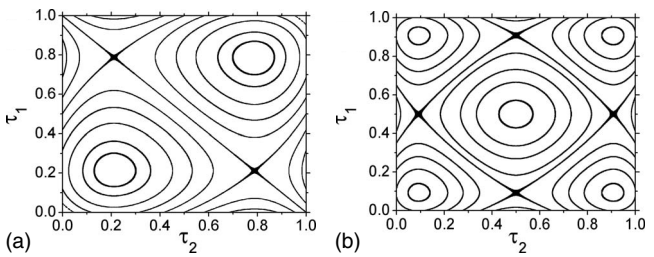

FIG. 10. Level curves determined by the Levitov-Lesovic formula, Eq. (1), with $N=2$ and increasing values of (a) the third CTC, q_3, and (b) the fourth CTC, q_4.

$$P_m^G(q_m) = \sum_{j=1}^{m} \frac{1}{\left|\frac{df_m}{d\tau}(\tau_j^*)\right|} \int_0^1 d\tau \delta(\tau - \tau_j^*), \tag{27}$$

where τ_j^* are roots of the polynomial equation $q_m - f_m(\tau) = 0$. Varying q_m, some roots can enter or leave the interval $[0,1]$, thus generating nonanalyticities in P_m^G. For arbitrary N, let $\mathcal{Z} = \{\tau_i^*\}_{i=1}^l$, with $\tau_i^* \in [0,1]$, denote the set of the l roots of the first derivative of $f_m(\tau)$. Since the dimension of the elements that can be touched takes values from 1 to $N-1$, the special values of q_m obtained from all the conditions explained previously must satisfy the relation

$$q_m^* = \sum_{i=1}^{l} \kappa_i f_m(\tau_i^*) \tag{28}$$

where

$$0 \leq \sum_{i=1}^{l} \kappa_i \leq N \tag{29}$$

To be more explicit, let us calculate the special values q_m^* for the second, third and fourth CTC when $N > 1$. In the shot-noise case $\mathcal{Z} = \{1/2\}$ and $f_2(1/2) = 1/4$. From Eqs. (29), it is easy to see that $q_2^* = \kappa/4$ where $0 \leq \kappa \leq N$, in agreement with Ref. 9. For the third CTC $\mathcal{Z} = \{1/2 \pm \sqrt{3}/6\}$, $f_3(1/2 \pm \sqrt{3}/6) = \mp\sqrt{3}/18$ and so, we have $q_3^* = (\kappa_1 - \kappa_2)\sqrt{3}/18$, where $0 \leq \kappa_1 + \kappa_2 \leq N$. Analogously, we have for the fourth CTC $\mathcal{Z} = \{1/2, 1/2 \pm 1/\sqrt{6}\}$, $f_4(1/2) = -1/8$, $f_4(1/2 \pm 1/\sqrt{6}) = 1/24$ and consequently $q_4^* = (-3\kappa_1 + \kappa_2 + \kappa_3)/24$ with $0 \leq \kappa_1 + \kappa_2 + \kappa_3 \leq N$.

The criteria established above locate all nonanalyticities of P_m that we found in our simulations for the first four CTC. We emphasize that the argument is mostly geometric with the number of open channels being the only physical input. This can be easily seen in Figs. 3 and 9, where nonanalyticities appear at the same values of q_m, regardless of the value of the barriers' transparency Γ or the symmetries of the cavity. However, it must be understood that the existence of the special points shown in Eq. (29) does not necessarily imply strong nonanaliticities in $P_m(q_m)$, since the joint distribution of transmission eigenvalues might smooth out the irregularity and also because the discontinuity in $P_m^G(q_m)$ may turn out to be very weak. This is particularly evident in the semiclassical regime where the number of open channels is large and a self-averaging takes place turning all distributions into Gaussians, albeit in this case nonanalyticities of a different kind have recently been shown to appear[6] both in the conductance and in the shot-noise power distributions. The possible special points of the first four CTC distributions according to the above described criteria are explicitly exhibited in the Appendix B.

VI. SUMMARY AND CONCLUSIONS

We presented a detailed study of the most relevant features of the distributions of the first four charge-transfer cumulants (CTCs) of a chaotic quantum dot with nonideal contacts. Physically, these distributions arise from the underlying spatial quantum coherence of the charge transport through the device. Our numerical analysis was performed via simulations based on three different algorithms. We observed two striking features in the extreme quantum limit: an approximate scaling law for conductance distributions and the appearance of a finite number of nonanalytical points in some CTC distributions. These nonanalyticities have been given a simple geometrical interpretation, which allowed for a precise determination of its position. Recent remarkable advances in the measurement techniques of high order CTC (Refs. 36 and 37) give us hope that some of our predictions might be experimentally verified in the future. The proper separation of quantum noise from other sources of noise within the experimental resolution is of course one of the biggest technical challenges. Particularly subtle is the proper control over dephasing effects, which may have several physical origins, including electron-electron interactions, and provides a natural drift toward Gaussian CTC distributions even in the extreme quantum limit.[10] Besides contributing to dephasing, electron-electron interactions can also have a sizable effect in the phase-coherent regime by affecting the skewness (third cumulant) of the conductance distribution, as observed by Mohanty and Webb in quasi-one-dimensional gold wires.[38] In the random-matrix description of open quantum dots, the effects of long-range Coulomb interactions can be implemented via capacitive couplings, as described in detail in Ref. 17.

We can envisage several ways to extend our work: the normal-metal terminals can be replaced by superconducting or ferromagnetic ones, the number of terminals can be increased, the single dot can be replaced by a network of dots of arbitrary topology, external fields can be introduced to drive the system to crossover regimes, dephasing can be modeled by fictitious terminals or stubs, and so on. Our central message is that the extreme quantum limit of mesoscopic transport contains important nonperturbative physics and appropriate tools to extract this information, numerical or analytical, still needs to be developed and constitutes a big challenge to the physicists working on this field.

ACKNOWLEDGMENT

This work was partially supported by CNPq (Brazilian Agency).

APPENDIX A: COMPARISON BETWEEN THE SAMPLING METHODS

In this work we implemented three sampling methods (MW, ST, and TM) to generate realizations of the scattering matrix of an open chaotic cavity with nonideal contacts. The realizations were generated by running a FORTRAN code on a CPU with a clock rate of 2.6 GHz under a GNU/Linux operating system. We shall now compare these methods assuming, for simplicity, that the system consists of a chaotic cavity with symmetric contacts. The main numerical difficulty in the MW method comes from the fact that the number of resonance levels M inside the cavity must be very large in order to generate the Poison kernel. Nevertheless, the use of

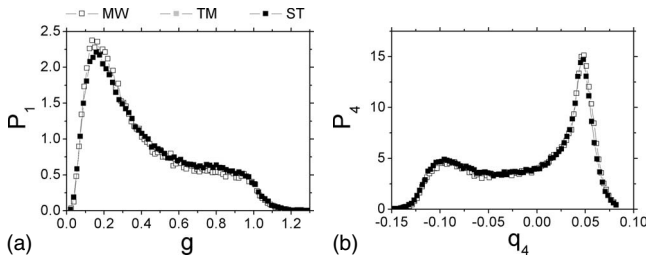

FIG. 11. Distributions of the conductance and the fourth CTC of a chaotic quantum dot with two scattering channels in each lead, barriers' transparency $\Gamma=0.4$ and $\beta=4$ using the three numerical methods explained in the text with 10^5 realizations.

10^5 realizations and the "rule of thumb" $M=4N$ is enough to produce at least 98% of accuracy in the calculations of the average conductance for ideal contacts and we have adopted these as a standard for all MW simulations. Notwithstanding this finite M approximation, Fig. 11 shows that the distributions obtained from the MW method are very close to the distributions obtained from the TM and ST methods, which can be shown to have only the usual statistical and numerical errors.

We observed that the processing time per realizations T_{CPU} grows with the number of channels according to the following power law:

$$T_{\mathrm{CPU}}(N) = \vartheta N^{\gamma}. \tag{A1}$$

Using estimated values of the parameters ϑ and γ we analyzed the efficiency of the methods, with regard to the processing time, and we concluded that the ST method is universally the most efficient. We can define a measure of the efficiency of the ST method relative to the MW or TM methods as follows:

$$\eta \equiv \frac{T_{\mathrm{CPU}}^{(\mathrm{MW\ or\ TM})}}{T_{\mathrm{CPU}}^{(\mathrm{ST})}} - 1. \tag{A2}$$

In Fig. 12 we show that for $1 \leq N \leq 30$ the efficiency of the ST method is between 7.5% and 32.5%, relative to TM, and between 150% and 310%, relative to MW.

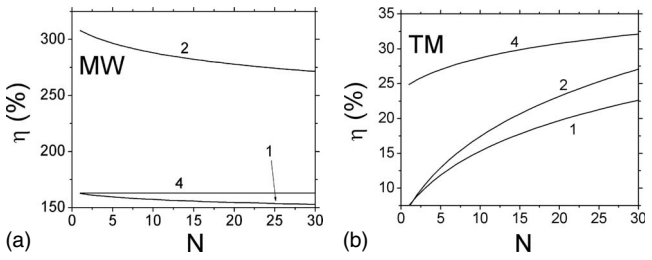

FIG. 12. Number of channels dependence of the efficiency of the ST method relative to the MW and TM methods based on Eq. (A2). The numbers labeling the curves are the values of β.

APPENDIX B: SPECIAL VALUES OF THE CUMULANTS

Define $\mathbb{Q}_{m,N}$ as the set of values of q_m, with $N=\min(N_1,N_2)$, at which a nonanalyticity may appear in the corresponding distribution. From the geometrical analysis explained in Sec. V, the possible values of $\mathbb{Q}_{m,N}$ for the first four CTC are given by

$$\mathbb{Q}_{1,N} = \{0,1,\ldots,N\},$$

$$\mathbb{Q}_{2,N} = \{0,1/4,\ldots,N/4\},$$

$$\mathbb{Q}_{3,N} = \{0,\pm\sqrt{3}/18,\ldots,\pm\sqrt{3}N/18\},$$

$$\mathbb{Q}_{4,1} = \{-1/8,0,1/24\},$$

$$\mathbb{Q}_{4,2} = \mathbb{Q}_{4,1} \cup \{-1/4,-1/12,1/12\},$$

$$\mathbb{Q}_{4,3} = \mathbb{Q}_{4,2} \cup \{-3/8,-5/24,-1/24,1/8\},$$

$$\mathbb{Q}_{4,4} = \mathbb{Q}_{4,3} \cup \{-1/2,-1/3,-1/6,1/6\},$$

$$\mathbb{Q}_{4,5} = \mathbb{Q}_{4,4} \cup \{-5/8,-11/24,-7/24,5/24\},$$

$$\mathbb{Q}_{4,6} = \mathbb{Q}_{4,5} \cup \{-3/4,-7/12,-5/12,1/4\},$$

$$\mathbb{Q}_{4,7} = \mathbb{Q}_{4,6} \cup \{-21/24,-17/24,-13/24,7/24\},$$

$$\mathbb{Q}_{4,8} = \mathbb{Q}_{4,7} \cup \{-1,-5/6,-2/3,1/3\},$$

$$\mathbb{Q}_{4,9} = \mathbb{Q}_{4,8} \cup \{-9/8,-23/24,-19/24,3/8\},$$

$$\mathbb{Q}_{4,10} = \mathbb{Q}_{4,9} \cup \{-5/4,-13/12,-11/12,5/12\}.$$

[1] F. Lefloch, C. Hoffmann, M. Sanquer, and D. Quirion, Phys. Rev. Lett. **90**, 067002 (2003).
[2] L. Saminadayar, D. C. Glattli, Y. Jin, and B. Etienne, Phys. Rev. Lett. **79**, 2526 (1997).
[3] A. H. Steinbach, J. M. Martinis, and M. H. Devoret, Phys. Rev. Lett. **76**, 3806 (1996); R. J. Schoelkopf, P. J. Burke, A. A. Kozhevnikov, D. E. Prober, and M. J. Rooks, *ibid.* **78**, 3370 (1997).
[4] G. Burkard, D. Loss, and E. V. Sukhorukov, Phys. Rev. B **61**, R16303 (2000).
[5] L. S. Levitov and G. B. Lesovik, Pis'ma Zh. Eksp. Teor. Fiz. **58**, 225 (1993) [JETP Lett. **58**, 230 (1993)]; L. S. Levitov, H. W. Lee, and G. B. Lesovik, J. Math. Phys. **37**, 4845 (1996); L. S. Levitov, in *Quantum Noise in Mesoscopic Systems*, edited by Yu. V. Nazarov (Kluwer, Dordrecht, 2003).
[6] P. Vivo, S. N. Majumdar, and O. Bohigas, Phys. Rev. Lett. **101**, 216809 (2008).
[7] V. A. Osipov and E. Kanzieper, Phys. Rev. Lett. **101**, 176804 (2008).
[8] H. U. Baranger and P. A. Mello, Phys. Rev. Lett. **73**, 142 (1994).

[9] H.-J. Sommers, W. Wieczorek, and D. V. Savin, Acta Phys. Pol. A **112**, 691 (2007).
[10] A. G. Huibers, S. R. Patel, C. M. Marcus, P. W. Brouwer, C. I. Duruöz, and J. S. Harris, Phys. Rev. Lett. **81**, 1917 (1998).
[11] K. A. Muttalib, P. Wölfle, A. García-Martín, and V. A. Gopar, Europhys. Lett. **61**, 95 (2003).
[12] K. A. Muttalib and P. Wölfle, Phys. Rev. Lett. **83**, 3013 (1999).
[13] P. Markos, Phys. Rev. Lett. **83**, 588 (1999).
[14] A. García-Martín and J. J. Sáenz, Phys. Rev. Lett. **87**, 116603 (2001).
[15] Yu. V. Nazarov, Superlattices Microstruct. **25**, 1221 (1999).
[16] P. W. Brouwer and C. W. J. Beenakker, J. Math. Phys. **37**, 4904 (1996).
[17] J. N. Kupferschmidt and P. W. Brouwer, Phys. Rev. B **78**, 125313 (2008).
[18] K. B. Efetov, *Supersymmetry in Disorder and Chaos* (Cambridge University Press, Cambridge, 1997).
[19] G. C. Duarte-Filho, A. F. Macedo-Junior, and A. M. S. Macêdo, Phys. Rev. B **76**, 075342 (2007).
[20] D. V. Savin, H.-J. Sommers, and W. Wieczorek, Phys. Rev. B **77**, 125332 (2008).
[21] M. Novaes, Phys. Rev. B **75**, 073304 (2007); **78**, 035337 (2008).
[22] J. G. G. S. Ramos, A. L. R. Barbosa, and A. M. S. Macêdo, Phys. Rev. B **78**, 235305 (2008).
[23] M. L. Metha, *Random Matrices* (Academic, New York, 1991).
[24] F. Haake, *Quantum Signatures of Chaos* (Springer, Berlin, 1991).
[25] C. W. J. Beenakker, Rev. Mod. Phys. **69**, 731 (1997).
[26] J. J. M. Verbaarschot, H. A. Weidenmüller, and M. R. Zirnbauer, Phys. Rep. **129**, 367 (1985).
[27] A. M. S. Macêdo, Phys. Rev. B **63**, 115309 (2001).
[28] P. W. Brouwer, Phys. Rev. B **51**, 016878 (1995).
[29] P. A. Mello and N. Kumar, *Quantum Transport in Mesoscopic Systems: Complexity and Statistical Fluctuations* (Oxford University Press, New York, 2004).
[30] A. Hurwitz, Nachr. Ges. Wiss. Goettingen, Math.-Phys. Kl. **71**, 309 (1898).
[31] K. Zyczkowski and M. Kus, J. Phys. A **27**, 4235 (1994).
[32] P. W. Brouwer and C. W. J. Beenakker, Phys. Rev. B **50**, 11263 (1994).
[33] J. G. G. S. Ramos, F. A. G. Almeida, and A. M. S. Macêdo (unpublished).
[34] S. Kullback and R. Leibler, Ann. Math. Stat. **22**, 79 (1951).
[35] L. Van Hove, Phys. Rev. **89**, 1189 (1953).
[36] S. Gustavsson, R. Leturcq, B. Simovic, R. Schleser, T. Ihn, P. Studerus, K. Ensslin, D. C. Driscoll, and A. C. Gossard, Phys. Rev. Lett. **96**, 076605 (2006).
[37] S. Gustavsson, R. Leturcq, T. Ihn, K. Ensslin, M. Reinwald, and W. Wegscheider, Phys. Rev. B **75**, 075314 (2007).
[38] P. Mohanty and R. A. Webb, Phys. Rev. Lett. **88**, 146601 (2002).